CNRS

Centre National de la Recherche Scientifique

INFN

Istituto Nazionale di Fisica Nucleare

Virgo+MS sensitivity curve

VIR-0639B-09

Date: Tuesday, 10 November 2009

Paola Puppo

VIRGO * A joint CNRS-INFN Project
Via E. Amaldi, I-56021 – S. Stefano a Macerata - 56021 Cascina, Italia.
Secretariat: Telephone.(39) 050 752 521 * FAX.(39) 050 752 550 * e-mail virgo@virgo.infn.it

Table of contents

1 Introduction

The fundamental noise sources in the interferometric gravitational wave antenna are determined by its conceptual design and they are used to define the ultimate sensitivity of the detector.
In this note we will describe all those contributions which are important for evaluate the sensitivity curve of the Virgo+ detector with and without the Monolithic Suspensions and we will refer to the 'Virgo sensitivity curve' paper [1] for those noise sources which do not change with the Virgo+ updates.
The parameters used for the computation are listed in the final section (7) of this note.

2 Seismic Noise

On the Virgo site the measured seismic spectral amplitude is given by :

(1.1) $$\tilde{x}_{seism}(\nu) \approx \frac{A_o}{\nu^2} \left[m/\sqrt{Hz} \right]$$

where $A_o = 1.5 \cdot 10^{-7} \left[m \right]$, as reported in the note [2]. This noise is filtered by the superattenuator (SA) chain providing the horizontal attenuation of a cascade of $N = 5$ pendula with a fundamental frequency of $\nu_o = 0.6\ Hz$ which in the off-resonance zone is:

(1.2) $$\frac{x(\nu)}{\tilde{x}_{seism}(\nu)} = \left(\frac{\nu_o}{\nu} \right)^{2N}$$

The complete response of the SA deals with the horizontal and vertical transfer functions of such a system which were calculated by A. Viceré giving the equivalent noise term due to the seismic displacement:

(1.3) $$h_{seism}(\nu) = \frac{2}{L_{arm}} \sqrt{\left[HTF(\nu) \right]^2 + \left[\theta_o VTF(\nu) \right]^2} \tilde{x}_{seism}(\nu)$$

The parameter $\theta_o = L/2R_E$ is the vertical to horizontal noise coupling given by the earth curvature.
Thanks to the the SA suspension, this noise is negligible in the Virgo sensitivity bandwidth which is limited by the suspension thermal noise above 10 Hz.

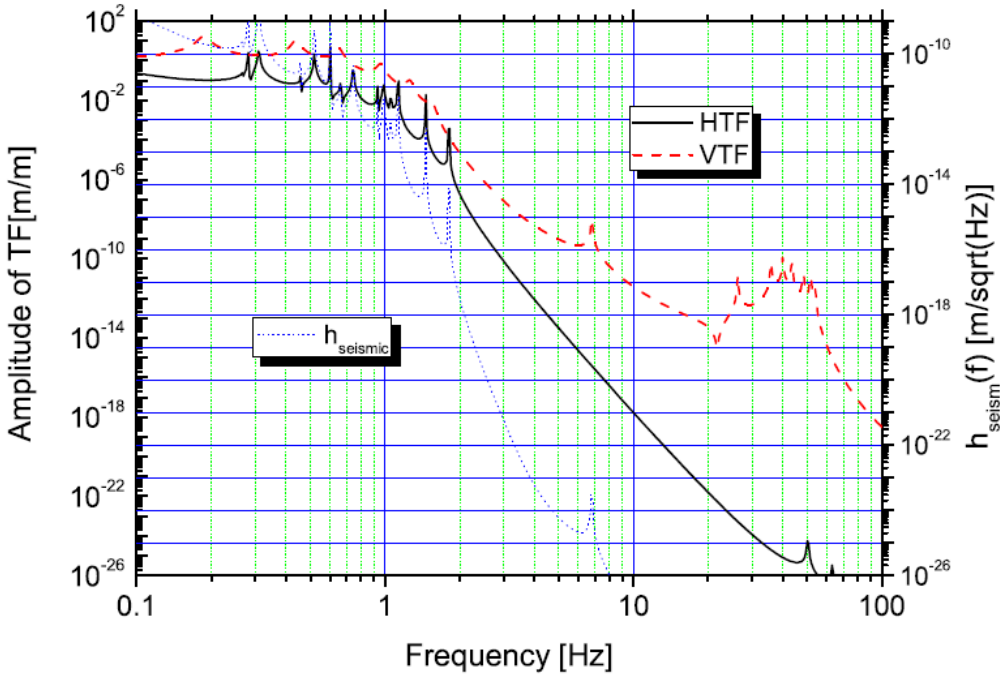

Figure 1: (From reference **(1)**) Horizontal (black) and vertical (dotted blue) transfer function of the Virgo SA. The seismic noise contribution (dotted blue).

3 The Suspension Thermal noise

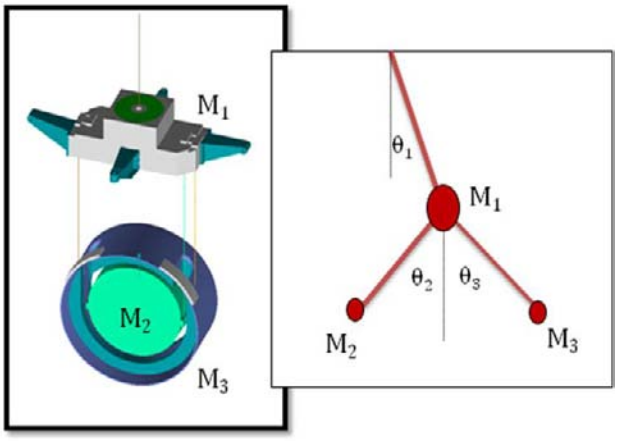

Figure 3-1: The Last Stage suspension and its pendulum equivalent scheme. M_1: Marionette; M_2: Mirror; M_3: Recoil Mass.

In the suspensions thermal noise there are three contributions :

- the pendulum thermal noise;
- the vertical thermal noise reduced by the Θ_o coupling factor;
- the violin modes thermal noise;

giving an overall expression for the strain:

$$h_{LSS}(\nu) = \frac{2}{L}\sqrt{\left\langle x_{pend}(\nu)\right\rangle^2 + \Theta_o^2\left\langle x_{vert}(\nu)\right\rangle^2 + \left\langle x_{viol}(\nu)\right\rangle^2} \tag{1.4}$$

The full theoretical treatments of the three contributions can be found on the note[4] (the PPP model), in which they were calculated taking into account the whole last stage suspension system including the pendulum stages of the marionette and the recoil mass[5]. In the off-resonance high frequency region, the mechanical losses of the recoil mass and mainly of the marionette suspensions can give non negligible contributions which induce the overall thermal noise curve to be different from the simple mirror curve. This effect becomes more evident as soon as the mirror pendulum losses are small like in the case with the Monolithic Suspensions (MS) or for Advanced Virgo [3]. For this reason the losses of all the three stages of the suspensions are included in the model.

3.1 The mechanical losses of the pendulum stage

In the model each uncoupled pendulum stage is described by the transfer function:

$$H_i(\omega) = \frac{1}{m_i}\frac{1}{\left(\omega^2 - \omega_{oi}^2\right) + i\omega_{oi}^2\left(\Phi_i(\omega) + \left(\frac{\omega}{\omega_{oi}}\right)\frac{1}{Q_i}\right)} \tag{1.5}$$

where m_i is the mass suspended to the wire and:

$$\omega_{oi}^2 = \omega_{ogi}^2 + \omega_{owi}^2$$

$$\omega_{ogi}^2 = \frac{g}{L_i} \quad ; \quad \omega_{owi}^2 = \frac{k_{eli}}{m_i} = \frac{2n_{wi}\sqrt{T_i Y_{wi} I_2^{(i)}}}{m_i} \tag{1.6}$$

T_i is the wire tension, n_{wi} the number of suspension wires of the i_{th} stage, and $I_2^{(i)} = (1/4)\pi r_{wi}^4$ is the area moment of inertia of the wire.

The overall structural loss angle of the pendulum can be written as:

$$\Phi_i(\omega) = D_{F_i}^{-1}(\Phi_{wi} + \Phi_e^{(i)} + \Phi_{te}^{(i)}(\omega)) \tag{1.7}$$

where $D_{F_i} = \frac{1}{L_i}\sqrt{\frac{4Y_{wi}I_2^{(i)}}{m_i g}}$ is the pendulum dilution factor defined as the ratio between the elastic energy stored in the wire (due to its elastic restoring force) and the total oscillation energy.

Each loss contribution contains the material loss angle Φ_{wi}, the thermoelastic $\Phi_{te}^{(i)}(\nu)$ and the eccess loss angle $\Phi_e^{(i)} = \Phi_{surf}^{(i)} + \Phi_{clamping}^{(i)} + \ldots$ of the wire.
The viscous losses due to eddy currents of the recoil mass, the residual gas and any other viscous process are included in the quality factor Q_i through the relation $\frac{1}{Q_i} = \frac{1}{Q_{eddy}} + \frac{1}{Q_{gas}} + \cdots$

3.1.1 The Thermoelastic losses

The thermoelastic losses model, including also the non-linear thermoelastic contribution [6] is given by the formula:

$$\Phi_{te}(\omega) = \Delta \frac{\omega\tau_{mat}}{1+(\omega\tau_{mat})^2}$$

(1.8)

$$\Delta = \frac{Y_{mat}}{C_{mat}\rho_{mat}}\left(\alpha_{mat} - \beta_{mat}\frac{\Lambda}{Y_{mat}\pi r_w^2}\right)^2 T; \quad \beta_{mat} = \frac{1}{Y_{mat}}\frac{dY_{mat}}{dT}; \quad \tau_{mat} = \frac{C_{mat}\rho_{mat}}{2\pi k_{mat}}\frac{(2r_w)^2}{2.16}$$

the τ_{mat} parameter sets the position of the maximum peak of the thermoelastic losses of a given wire.
This parameter can be optimized by the choice of the material and the diameter of the suspension wire.

3.1.2 The residual gas damping

The residual gas damping represents an upper limit for the quality factor of the payload and is given by the formula:

$$Q_{gas} = 4\frac{M_i}{A_i}\frac{\omega_{oi}}{P_T}\sqrt{\frac{\pi k_B T}{8\mu_{H_2}}} \tag{1.9}$$

where μ_{H_2} is the H_2 molecule mass and A_i is the section of the mass which is mainly exposed to the residual gas scattering. For the mirror the quality factor limit is $(Q_{gas})_{mirror} \simeq 2.3\cdot 10^{13}$, for the marionette (see Figure 3) and for the recoil mass (see Figure 4) is $(Q_{gas}) \simeq 10^{14}$.

3.1.3 The eddy currents damping

It is well understood that the viscous damping due to the eddy currents between the recoil mass and the mirror sets a limit to their quality factor.
This limit was evaluated [7] and also measured in laboratory with the recoil mass presently used in Virgo [8]. The limiting Q is given by the formula:

$$Q_{eddy} = \frac{1}{n_m \Im}\frac{M\omega_{og}}{2\pi\left(\frac{3\mu_o\mu_m}{4\pi}\right)^2}\rho_{el} \tag{1.10}$$

where $\Im$ is a form factor that depends on the geometry of the system where the eddy currents flow, μ_m is the magnetic moment of the permanent magnet, ρ_{el} is the electrical resistivity of the reaction mass and n_m is the number of magnets on the mirror perimeter. The form factor is difficult to calculate because of the complex shape of the recoil mass, from the measurement was drawn to be $\Im = 585\ m^{-3}$.
Using the formula (1.10), an estimation of the quality factor for the recoil mass and the mirror in the Virgo+ set up (without MS) can be done. The present recoil mass is made of Al6063 having a resistivity of $\rho_{Al6063} = 3.14\cdot 10^{-8}\ \Omega\cdot\mathrm{m}$, we obtain $Q_{eddy}^{mirror} \simeq 2.3\cdot 10^7$ and $Q_{eddy}^{rm} \simeq 6.9\cdot 10^7$. These values represent an upper limit to the viscous quality factors in the Virgo payload.

In the case of the MS payload the recoil mass is composed by two main parts differently made of: and outer stainless steel AISI316L cylindric mass and an inner mass made of Tekapeek (CF30) carbon loaded, which is dielectric. Thanks to this new design the eddy currents coupling with the magnets is negligible.

3.1.4 The Mirror Monolithic Suspension

In the case of the MS the mirror is suspended with fused silica wires.
The wires upper clamps are hosted in stainless steel boxes providing a tight and safe coupling with the marionette body. The lower clamps provide the connection with the mirror lateral surface by means of fused silica 'ears' silicate bonded on its lateral surface (see Figure 3).

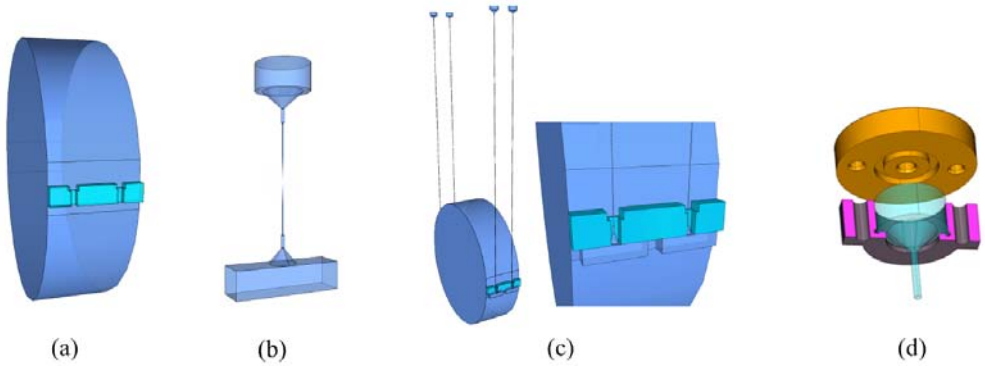

Figure 2: MS clamping system: (a) Mirror 'ears'; (b) FS wire clamps; (c) Lower clamping system; (d) Upper clamping system.

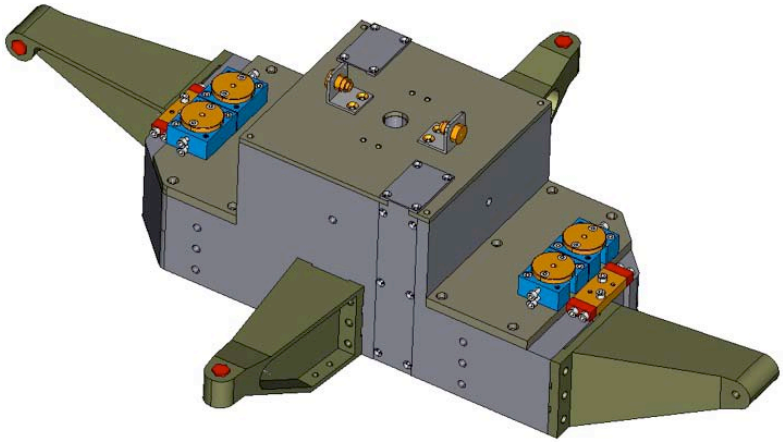

Figure 3: Marionetta of the MS payload.

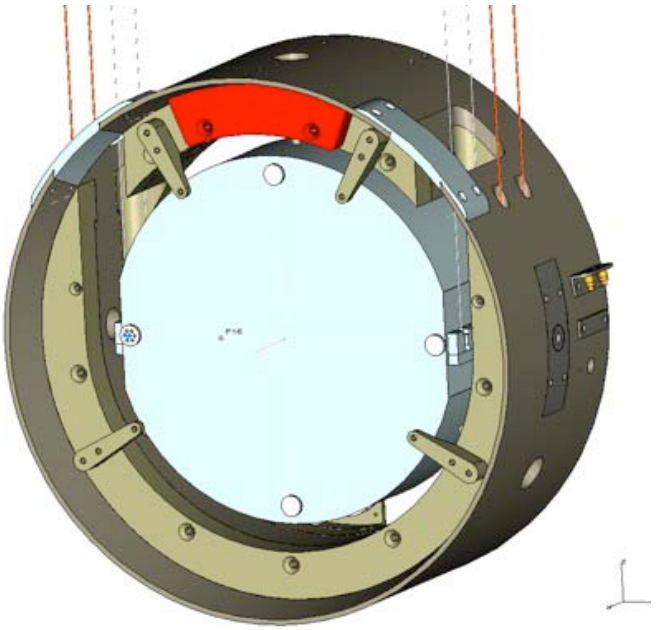

Figure 4: Recoil Mass of the MS suspensions

3.1.4.1 The Clamp Losses of the monolithic suspensions

In the case of the monolithic suspensions the measurements performed on the upper clamps has shown that their contribution is negligible [9].
As far as the lower clamps, the losses due to the bonded region of the ears can be evaluated as the fraction of elastic energy lost in the bonded zone during the pendulum oscillation [10]. The result, found with a FEM simulation, gives a negligible value of $\Phi_{ears} = 4.6 \times 10^{-13}$. as a consequence the overall losses Φ_{clamps} due to the upper and lower clamps are negligible in the model.

3.1.4.2 The Surface losses of the silica wires

The surface losses of the wires have been modeled by Gretarsson et al in the reference [11][12][13] and have been evaluated for the fused silica wires. The surface loss angle Φ_{surf} can be calculated as the fraction of elastic energy lost in surface zone involved in the bending during the oscillation. As a consequence it can be written as:

$$\Phi_e = \frac{W_{surf}}{W_{tot}} \Phi_{surf} = \Phi_{mat} \left(\mu_w \frac{d_s}{V_w / S_w} \right) = \Phi_{mat} \left(4 \frac{d_s}{d_w} \right) \tag{1.11}$$

where μ_w is a form factor equal to 2 for the cylindrical fibers, d_s is the dissipation depth which parametrizes the fiber size at which the surface damage becomes important. The quantities $V_w = L_w \pi r_w^2, S_w = L_w 2\pi r_w$ are the total volume and the surface of the fiber. This loss mechanism is present only in the pendulum modes.
In the case of Virgo+ with the MS the diameter of the wires is 285 μm: the surface loss angle is $\approx 1.8 \cdot 10^{-7}$.

Hence, at the pendulum frequency, the overall loss angle of the monolithic suspension is not influenced by the clamps and is $\Phi_{wire} \approx 10^{-6}$. As a consequence an overall loss angle of $\Phi_1 = D_F^{-1}(\Phi_{wire}) \approx 10^{-9}$ can be used for the silica wires.

3.1.5 The structural and viscous losses of the Virgo+ mirror pendulum (without the MS)

The suspension thermal noise of the Virgo sensitivity curve has been always computed considering a structural damping model, determined by a suspension wire loss angle of about $2 \cdot 10^{-4}$ [14] which was increased by an excess loss angle in order to agree with the pendulum Q of about $8 \cdot 10^5$ measured in a full scale prototype [15].

This interpretation of the quality factor as a structural or a viscous loss mechanism has been using the new PPP model compared with the measured Virgo sensitivity curve. From this comparison the eccess losses seem to dominate giving an overall loss angle $\Phi_1 = \left(D_F\right)^{-1} 1.5 \cdot 10^{-3}$ and an additional viscous damping $Q_{eddy} = 6 \cdot 10^7$ is introduced as a residual eddy current damping (M. Punturo logbook entry 22523).

The yielded eddy current losses can be compared with the measured one of $Q_{eddy} = 3 \cdot 10^7$ on the full scale prototype (see section 3.1.3). The small discrepancy between the two values can be explained by the measurements error in the extrapolation of residual eddy current effect from the comparison with noise curve.

However, in the comparison with the noise curve the value of $Q_{eddy} = 6 \cdot 10^7$ seems more reasonable.

3.1.6 The recoil mass and the marionette structural losses

In the PPP thermal noise model the recoil mass losses are not so important as the marionette ones. They are included in the model using the nominal wire properties. In Figure 6 the behaviour of the structural losses of the three stages are shown for the MS case.

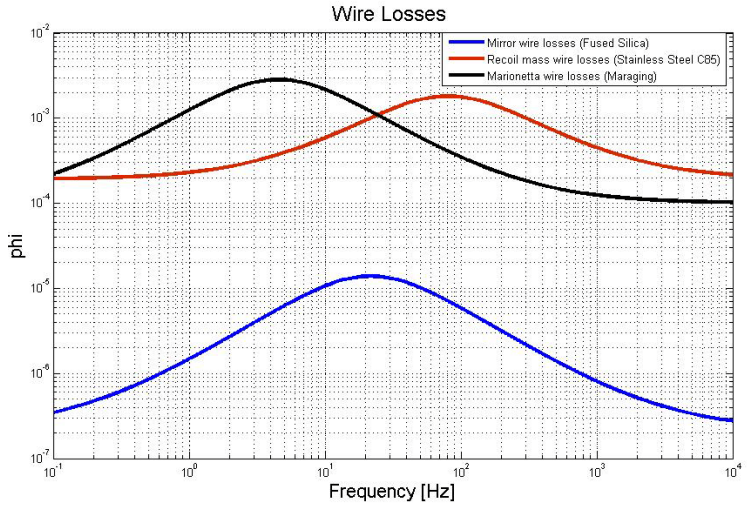

Figure 5: Overall loss factors of the wires in the Monolitic last stage suspension

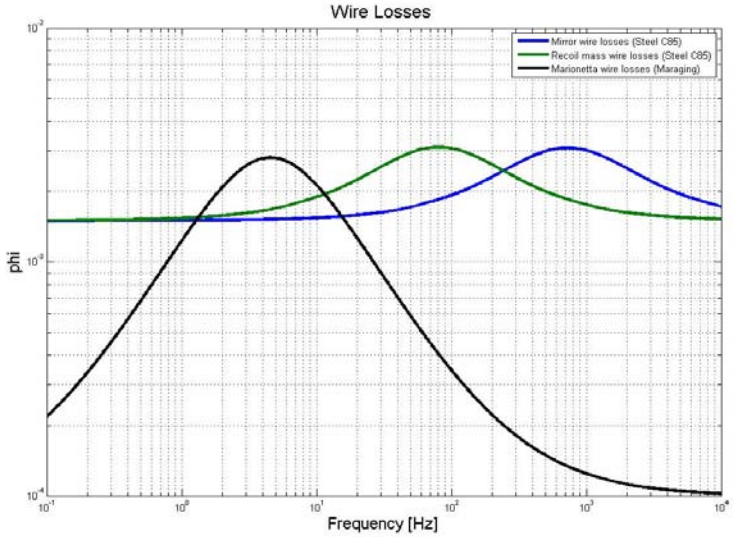

Figure 6: Overall loss factor of the suspension wires the Virgo+ without MS

3.1.7 The marionette pendulum losses

As mentioned at the beginning of the section, on the suspension thermal noise, the losses of the marionette pendulum stage are crucial for the correct estimation of the sensitivity curve at low frequency. It is not possible to have a direct measurement the marionetta losses when it is hung to the SA because in this configuration we can just measure the overall quality factor of the last stage pendulum modes, moreover its losses are quite influenced by the whole SA chain.
The experimental evidence is that the quality factors of the modes are influenced by the quality factors of the SA chain and the modes have a value of about 30-50. However, from the measurements of the quality factors performed on the monolithic suspension prototype we can set a lower limit to the marionette quality factor which is 1000. This factor, is measured on the monolithic suspension setup, in air and without the presence of the filter 7. The result suggests that it is possible to decrease the viscous losses of the marionette when it is mounted on the SA chain, by trying to improve its coupling to the filter 7. To be conservative we reckon that it is possible to improve by a factor 10 the losses by reaching a marionette quality factor of 300. Further investigations are needed for better understand this aspect. As a comparison, in figure we show the Virgo+ thermal noise with Q_{mario}=100 compared with Q_{mario}=300 and Q_{mario}=50.

The affected region is below 100 Hz and the quality factor of the marionette can influence considerably the BBH view distance.

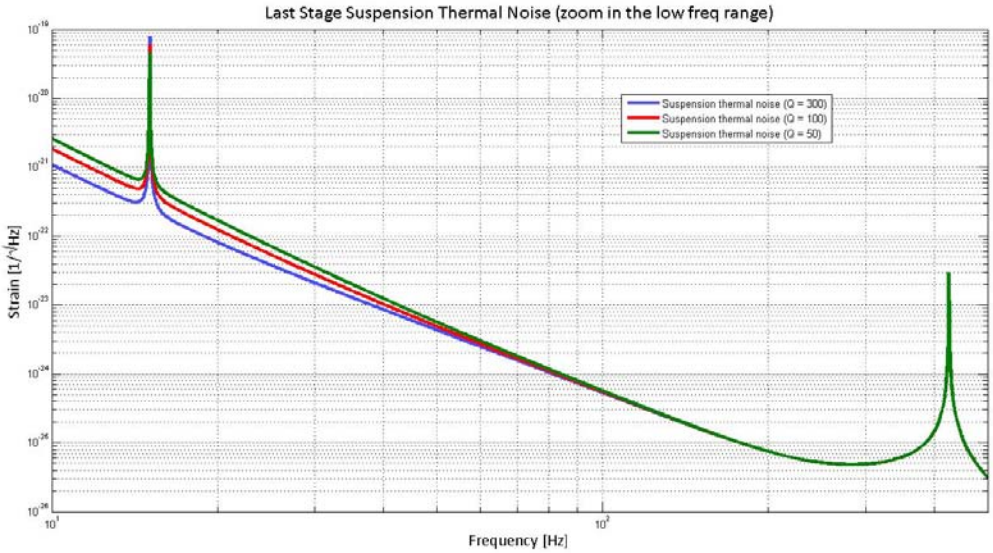

Figure 7: Monolithic Last Stage Suspensions Thermal noise with 3 possible viscous dissipations on the marionette.

3.2 The Vertical thermal noise

The vertical noise is coupled to the horizontal motion of the last stage suspensions by the fraction θ_o, by means of the formula (1.4). The full expression has been calculated with the new PPP model [4] for the last stage suspension. Each stage is seen as a vertical oscillator with a the frequency:

$$\omega_{vj}^2 = \begin{cases} \dfrac{k_j}{m_j} & ; \quad j = 1,2 \\ (2\pi \cdot 0.4)^2 & ; \quad j = 3 \text{ (marionette)} \end{cases} \qquad k_j = n_j Y_j \frac{\pi r_j^2}{L_j} \tag{1.12}$$

where the vertical frequency of the marionette is dominated by the softness of the magnetic anti-spring suspension system (0.4 Hz of vertical frequency).
The losses of the wires are shown in the figures Figure 6 and Figure 7 and they are not diluted by the factor D_{F_i} like in the case of the pendulum oscillations.

(1.13) $$H_{v_i}(\omega) = \frac{1}{m_i} \frac{1}{\left(\omega^2 - \omega_{vi}^2\right) + i\omega_{vi}^2 \left(\Phi_{iv}(\omega) + \left(\frac{\omega}{\omega_{vi}}\right)\frac{1}{Q_{vi}} \right)}$$

with $\Phi_{iv}(\omega) = (\Phi_{wi} + \Phi_e^{(i)} + \Phi_{te}^{(i)}(\omega))$.

3.3 The Mirror Thermal

The expression of the mirror thermal noise can be evaluated by using the Fluctuation Dissipation Theorem which, in the frequency range below the mirror mode frequency, leads to the Levin following formula [22] :

(1.14) $$\left\langle x_{therm}(\nu) \right\rangle^2 = \frac{2k_B T}{\pi \nu} U \Phi_{mirr}$$

where the mirror loss angle includes the substrate, the coating losses and the losses due to the presence of the silicate bonded ears on its lateral sides, by the relation: $\Phi_{mirr} = \Phi_{substr} + \Phi_{coating} + \Phi_{Bonding}$. The quantity U is the elastic energy of the mirror weighted by the use of the Gaussian beam readout observable. This calculation is valid in the region below the mirror resonances and it does not include them.
The detailed expression of such a noise can be found in the note [3]. The formula of the mirrors thermal noise in terms of the strain can be written as:

(1.15) $$h_{therm}(\nu) = \frac{1}{L}\sqrt{2\left[\left\langle x_{therm}(\nu)\right\rangle^2\right]_{Near} + 2\left[\left\langle x_{therm}(\nu)\right\rangle^2\right]_{Far}}$$

where the near and the far mirrors give a separate contributions due the different size of the Gaussian beams.

The Loss angle of the mirror substrates

In the present Virgo interferometer (Virgo+ without MS) the near mirror substrates are made of Suprasil and the far mirrors are made of Herasil.

The experimental bulk loss angles of such materials are $\left[\Phi_{bulk}\right]_{NM\,(Suprasil)} = 10^{-7}$ and $\left[\Phi_{bulk}\right]_{FM\,(Herasil)} = 1.3 \cdot 10^{-6}$.

For the Suprasil a model has been developed by Steve Penn and his collaborators [16] which rely on the experimental measurements performed on several samples of different kinds of Suprasil. They have fitted their data with the following equation:

(1.16) $$\Phi_{sub}(\nu) = \Phi_e^{sub} + C_2 \nu^{C_3}; \qquad \Phi_e^{sub} = C_1\left(\frac{S}{V}\right)$$

For Virgo+ with MS all the substrates (near and far mirrors) will be made of Suprasil 312 (more pure than that one of Virgo). The Penn's measured parameters for this material are: $C_1 = 6.5 \cdot 10^{-12} m, C_2 = 7.6 \cdot 10^{-12}, C_3 = 0.77$, obtaining a loss angle of about 10^{-9}at 1kHz.

Mechanical Losses of the coating

The coating are composed by several layers of high and low refraction index materials so that the wanted reflectivity is obtained. The mechanical losses of such materials give loss angles which are quite high respect to the substrate ones. The full formula of the coating losses, can be found on the reference [3]. It takes into account the coating geometrical and structural properties and gives:

Virgo

Near Mirror coating overall loss angle: $[\Phi_{\text{coat}}]_{\text{NM}} = 3.7\ 10^{-8}$

Far Mirror coating overall loss angle: $[\Phi_{\text{coat}}]_{\text{FM}} = 3.4\ 10^{-8}$

Virgo+MS

Near Mirror coating overall loss angle: $[\Phi_{\text{coat}}]_{\text{NM}} = 2.7\ 10^{-8}$

Far Mirror coating overall loss angle: $[\Phi_{\text{coat}}]_{\text{FM}} = 2.5\ 10^{-8}$

Mechanical Losses due to the bonded earsin the MS

The losses of the bonded region of the monolithic suspension must be included in the calculation of the mirror thermal noise.

They can be calculated as the fraction of elastic energy lost in the bonded zone during the mirror oscillation. For each mirror mode n they can be written as:

$$\Phi_{bonding}^{(n)} = \frac{W_{bonding}^{(n)}}{W_{tot}^{(n)}} \Phi_{sibo} \quad (1.17)$$

where Φ_{sibo} is the average bond loss. This number depends on the type of silicate bonding used and on the thickness of the bonded zone. Recently [17] the average bond losses were measured for the 61 nm thick bond giving $\Phi_{sibo} = 0.1$. The evaluation of the elastic energy fraction in the case of Virgo+ has been performed using the measured values and giving $\Phi_{bonding}^{(drum)} = 3.4 \times 10^{-9}$ for the mirror drum mode [10].

4 Thermo-Dynamical fluctuation of the mirror bulk and coating. Thermo-refractive noise of the coating

The fluctuations of the mirror and coating temperature with respect to the average value can be expressed with its variance $\delta T^2 \propto T^2$ related to the heat capacity of the materials [18]. They give rise to an equivalent strain noise proportional to the temperature and dependent on the thermal properties of the material.

The thermorefractive noise is another effect of the temperature fluctuation [19] which affects the refraction index of the coating layers through their dependence on temperature :

$$\beta_{low} = \beta_{SiO_2} = \frac{dn_{SiO_2}}{dT}; \qquad \beta_{high} = \beta_{Ta_2O_5} = \frac{dn_{Ta_2O_5}}{dT}$$

The full expression of these effects can be found in the reference [3].

5 The optical read-out noise

The quadratic sum of the shot noise and the radiation pressure noise is the read-out noise. Using the formalism of H.J.Kimble at al [20], this noise can be written in a more compact way, allowing also to insert the signal recycling cavity in the case of the Advanced interferometers.

We have :

$$h_{opt}(\omega) = \frac{h_{SQL}(\omega)}{\sqrt{2}} \sqrt{\frac{3}{2}\frac{1}{\mathrm{K}(\omega)\eta} + \mathrm{K}(\omega)}$$

$$h_{SQL}(\omega) = \sqrt{\frac{8\hbar}{M_m \omega^2 L^2}} \qquad \text{ITF Standard Quantum Limit}$$

$$\mathrm{K}(\omega) = \frac{I_{BS}}{I_{SQL}} \frac{2\gamma_{FP}^4}{\left(\gamma_{FP}^2 + \omega^2\right)\omega^2} \quad ; \quad \mathrm{I}_{SQL} = \frac{M_m L^2 \gamma_{FP}^4}{4 \cdot 2\pi \cdot (c/\lambda)} \quad ; \quad \mathrm{I}_{BS} = \mathrm{P}_{\mathrm{laser}} \cdot \mathrm{R}_C \quad ; \quad \gamma_{FP} = 2\pi \cdot f_{FP} = 2\pi \frac{c}{4L\,F}$$

(1.18)

where η is the photodiode efficiency, the factor $3/2$ has been evaluated by F. Bondu [21] for the Virgo modulation scheme.

6 Physical Constants

All of these physical constants are used for the calculation of the fundamental noises.

Physical Quantity	Symbol	Value	Units
Boltzmann Constant	k_b	$1.3807 \cdot 10^{-23}$	$J \cdot K^{-1}$

Planck Constant	h $\hbar$	$6.6261 \cdot 10^{-34}$ $1.0546 \cdot 10^{-34}$	$J \cdot s$
Gravitional acceleration	g	9.8	$m \cdot s^{-2}$
Speed of light in vacuum	c	$2.9979 \cdot 10^{8}$	$m \cdot s^{-1}$
Gravitational constant	G	$6.6726 \cdot 10^{-11}$	$m^3 s^{-2} kg^{-1}$
Earth Radius	R_E	$6370 \cdot 10^{3}$	m
Earth Density	ρ_E	2000	$kg \cdot m^{-3}$
Mass of the H_2 molecule	μ_{H_2}	$3.34765 \cdot 10^{-27}$	kg

7 Parameters of the interferometer Virgo+

In the following the geometrical, optical and material properties of the Virgo+ detector are given.

7.1 Interferometer infrastructure

Length of the harms: $L = 3000 \quad m$

Residual gas pressure: $P_r = 1.2 \cdot 10^{-7} \quad Pa$

Hydrogen molecule mass: $m_{H2} = 3.34765\ 10^{-27}\ \mathrm{kg}$

Temperature: $T = 290\ \mathrm{K}$

7.2 Laser

Laser Wavelength $\lambda = 1.064\ 10^{-6}\ \mathrm{m}$

Laser Power (injection system output) $P = 25\ \mathrm{W}$

7.3 Optics

PR Cavity Length $L_{PR} = 12\ \mathrm{m}$

Photo Detector Efficiency $\eta = 0.93$

For Virgo+ MS

Recycling Factor $R_C = 20$

Finesse $F = 150$

For Virgo+

Recycling Factor $R_C = 45$

Finesse $F = 50$

7.4 Beam

INPUT waist $w_N = 2.0\ \mathrm{cm}$

END waist $w_F = 5.5\ \mathrm{cm}$

7.5 Last Stage Suspension

Vertical-Horizontal x-Coupling.

This parameter can be estimated by taking into account the curvature of the earth by the formula $\Theta_o = L/(2R_E) = 2.35 \cdot 10^{-4}$. However this number gives just a lower limit and does not contain the precisions in the mechanics of the mirror suspensions. Several estimation has been done on the Virgo data using

two different techniques. One technique is to excite vertically the mirror suspension and to look at the mirror horizontal response, this gives a value very close to $2.35 \cdot 10^{-4}$. A second technique is to look at the amplitude of one of the vertical peeks on the noise curve and supposing this is thermal, to compare it with the prediction, this gives a value of $\Theta_o = 10^{-3}$. For each results the error should be evaluated.

In the calculation the value of $\Theta_o = 10^{-3}$ is used but a further investigation is needed.

7.5.1 Mirror suspended with silica wires (monolithic suspension)

End Mirror flats	$f_{END} = 100$ mm
Input Mirror flats	$f_{IN} = 50$ mm
Thickness	th = 100 mm
Mass of ears and anchors:	$m_{ears} = 110$ g
END mirror mass	$m_{END} = 20.1$ kg
INPUT mirror mass	$m_{INPUT} = 20.3$ kg
Wire length	$L_1 = 0.7$ m
Wire diameter	$d_1 = 285$ mm
Horizontal Viscous losses	no
Vertical Viscous losses	no

7.5.1.1 Silica properties

density	$\rho_{si} = 2.2\ 10^3$ kg/m^3
specific heat	$C_{si} = 772$ J/kg/K;
Poisson ratio	$\sigma_{si} = 0.17$
heat conductivity	$K_{si} = 1.38$; W/m/kg;
Thermal expansion	$\alpha_{si} = 5.1\ 10^{-7}$ m/m/K;

Young modulus vs temperature gradient Y_{si} =(69 + 0.0134 T) GPa=72.9 GPa [23]

Young modulus temperature gradient $\beta_{si}=(1/ Y_{si})(dY_{si}/dT) = 1.86\ 10^{-4}$ (1/K) [23]

loss angle	$\Phi_{si} = 3.3\ 10^{-8}$
Young Modulus	$Y_{si} = 7.27\ 10^{10}$ Pa
dissipation depth	Dissdepth = 200 μm

7.5.2 Mirror suspended with C85 wires

End Mirror flats	$f_{END} = 50$ mm
Input Mirror flats	$f_{IN} = 50$ mm
Thickness	th = 100 mm
END mirror mass	$m_{END} = 20.2$ kg
INPUT mirror mass	$m_{INPUT} = 20.2$ kg
Wire length	$L_1 = 0.7$ m
Wire diameter	$d_1 = 200$ mm
Horizontal Viscous losses	$6 \cdot 10^7$
Vertical Viscous losses	$6 \cdot 10^7$

7.5.3 Recoil mass suspended with c85 steel wires

Mass	$m_2 = 64$ kg
Electrical resistivity of AISI316L	$\rho_{el} = 7.51 \cdot 10^{-7}\ \Omega \cdot$m

Electrical resistivity of Al6063	$\rho_{el} = 3.14 \cdot 10^{-8}\ \Omega \cdot m$
Wire length	L_2 = 0.7 m
Wire diameter	d_2 = 600 μm
loss angle	$\Phi_{c85}^{virgo} = 1.5\ 10^{-3}$ (Michele's logbook entry)
Horizontal Viscous losses	$Q_{h2}=10^{10}$
Vertical Viscous losses	$Q_{v2}=10^{10}$

7.5.3.1 C85 steel (AISI1085) nominal properties

density	ρ_{c85} = 7.85 10^3 kg/m^3
specific heat	C_{c85} = 475 J/kg/K;
Poisson ratio	σ_{c85} =0.29
heat conductivity	K_{c85} = 50 W/m/K;
Thermal expansion	α_{c85} = 14 10^{-6} m/m/K;

Young modulus vs temperature gradient Y_{si} =(211 + 0.0357 T-1.1 10^{-4}) GPa=72.9 GPa [24]
Young modulus temperature gradient $\beta_{si}=(1/Y_{si})(dY_{si}/dT)$ = 1.8 10^{-5} (1/K) [24]

loss angle	Φ_{c85} =1.9 10^{-4}
Young Modulus	Y_{c85} = 2.1 10^{11} Pa
dissipation depth	$Dissdepth_{c85}$ = 0

7.5.4 Marionetta suspended with maraging steel wires

Mass	m_3 = 98 kg
Wire length	L_3 = 1.125 m
Wire diameter	d_3 = 1.85 mm
Horizontal Viscous losses	Q_{h3}=300
Vertical Viscous losses	Q_{v3}=300

7.5.4.1 Maraging steel (C-Type 250 UNS92890) properties

density	$\rho_{maraging}$ = 7.425 10^3 kg/m^3
Poisson ratio	$\sigma_{maraging}$ =0.311
specific heat	$C_{maraging}$ = 460 J/kg/K;
heat conductivity	$K_{maraging}$ = 24.6 W/m/K;
Thermal expansion	$\alpha_{maraging}$ = 17.9 10^{-6} m/m/K;

Young modulus temperature gradient $\beta_{si}=(1/Y_{si})(dY_{si}/dT)$ = -2.2 10^{-4} (1/K) [24]

loss angle	$\Phi_{maraging}$ = 10^{-4}
Young Modulus	$Y_{maraging}$ = 1.89 10^{11} Pa
dissipation depth	$Dissdepth_{maraging}$ = 0

7.6 Substrate and Coating

7.6.1 Mirror geometry

Diameter	$D_{mirror} = 350$ mm
Thickness	$th_{mirror} = 100$ mm
Mass	$M_m = 20.2$ *kg*

7.6.1.1 Substrate (SiO2, Suprasil 312) [25]

density	ρ_{sub} = 2.2 10^3 kg/m^3
Young Modulus	Y_{sub} = 7.27 10^{10} Pa
Poisson ratio	σ_{sub}=0.17
Thermal expansion	α_{sub} = 3.9 10^{-7} m/m/K
Refraction index temperature gradient	β_{sub} = 1.52 10^{-4} (1/K)
Refraction index	n_{sub} = 1.452

For Virgo+ without MS: $\left[\Phi_{bulk}\right]_{NM\,(Suprasil)} = 10^{-7}$ and $\left[\Phi_{bulk}\right]_{FM\,(Herasil)} = 1.3 \cdot 10^{-6}$.

For Virgo+ with MS: $C_1 = 6.5 \cdot 10^{-12} m, C_2 = 7.6 \cdot 10^{-12}, C_3 = 0.77$

7.6.2 Coating properties

Thicknesses

high index material on Near Mirror: $[d_{n1}]_{NM}$=0.71 10^{-6} m
low index material on Near Mirror: $[d_{n2}]_{NM}$=1.49 10^{-6} m
high index material on Far Mirror: $[d_{n1}]_{FM}$=2.13 10^{-6} m
low index material on Far Mirror: $[d_{n2}]_{FM}$=3.21 10^{-6} m
total thickness on Near Mirror: d_N=2.2 10^{-6} m
total thickness on Far Mirror: d_F=5.3 10^{-6} m

7.6.2.1 high index material: tantala (Ta_2O_5)

Young Modulus Y_{Ta} = 1.40 10^{11} Pa
Poisson ratio σ_{Ta}=0.26
Thermal expansion α_{Ta} = 3.6 10^{-6} m/m/K
Refraction index temperature gradient β_{Ta}= 1.4 10^{-5} (1/K)
loss angle Φ_{Ta} = 4.4 10^{-4}
refraction index n_{Ta} = 2.035

7.6.2.2 high index material: tantala (Ti:Ta_2O_5)

Young Modulus Y_{Ta} = 1.40 10^{11} Pa
Poisson ratio σ_{Ta}=0.26
Thermal expansion α_{Ta} = 3.6 10^{-6} m/m/K
Refraction index temperature gradient β_{Ta}= 1.4 10^{-5} (1/K)
loss angle Φ_{Ta} = 2 10^{-4}
refraction index n_{Ta} = 2.035

7.6.2.3 low index material: SiO_2

Young Modulus Y_{Low} = 7.2 10^{10} Pa
Poisson ratio $\sigma_{\mathbf{Low}}$=0.17
Thermal expansion $\alpha_{\mathbf{Low}}$ = 5.1 10^{-7} m/m/K
Refraction index temperature gradient $\beta_{\mathbf{Low}}$= 8 10^{-6} (1/K)
loss angle $\Phi_{\mathbf{Low}}$ = 5 10^{-5}
refraction index $n_{\mathbf{Low}}$ = 1.458

8 Conclusions

The two sensitivity curves without and with the Monolithic Suspensions and their comparison are shown in the Figure 9, Figure 10 and Figure 11. The difference between the curves in the high frequency range is explained by the different recycling factors ($R_C(V_+) = 45$ *and* $R_C(V_+MS) = 20$).

The following table shows the evaluations of the average sight ranges for the BNS and BBH inspirals.

Average sight range		
	BNS inspiral	BBH inspiral
Virgo +	13 MPc	44 Mpc
Virgo + with MS	47 MPc	394 MPc

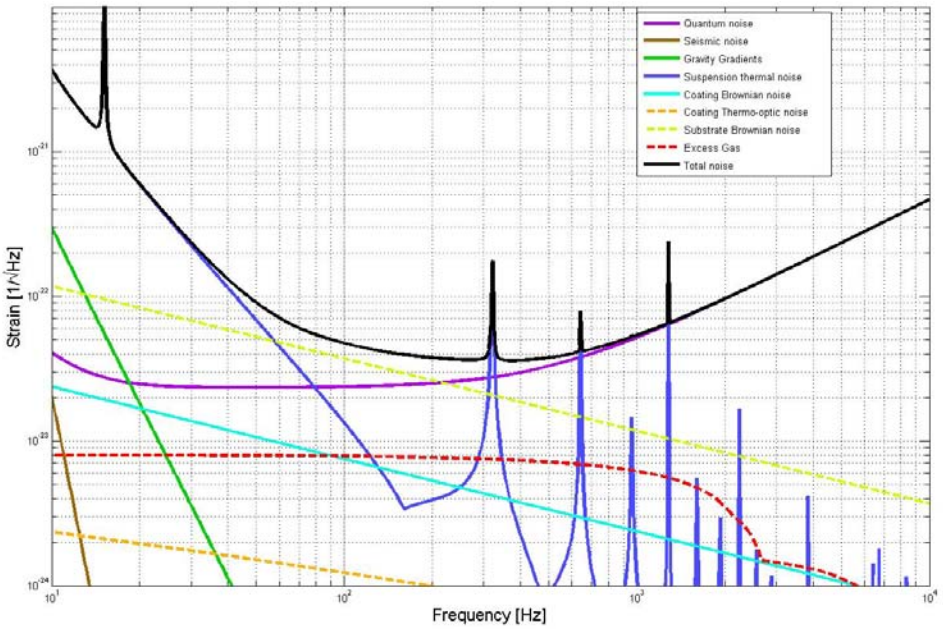

Figure 8: Virgo+ sensitivity curve (without MS)

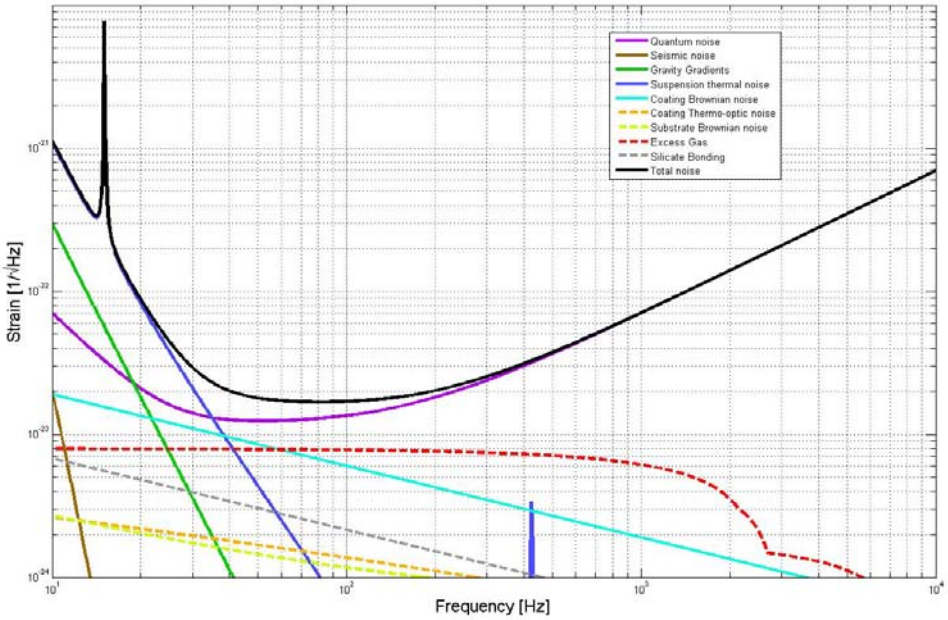

Figure 9: Virgo+ Sensitivity Curve (With MS)

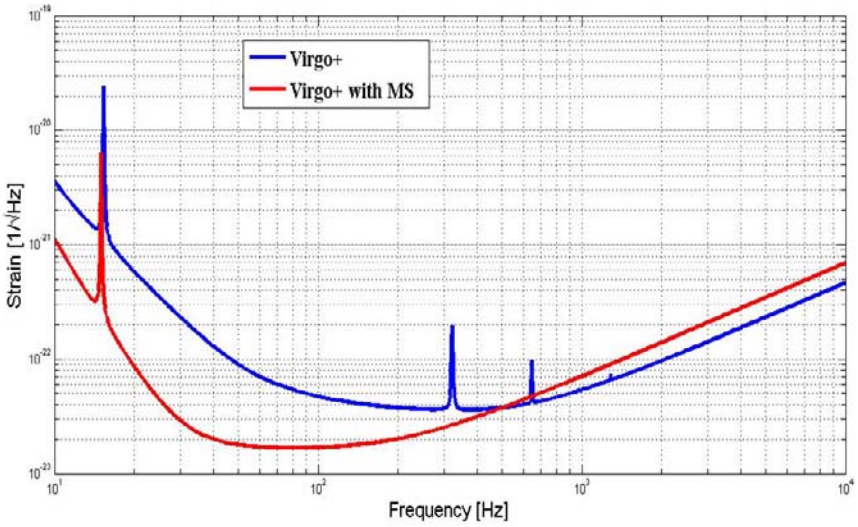

Figure 10: Virgo+ curves comparison. The difference in the high frequency range is explained by the different recycling factor (45 vs 20 of Virgo+ with MS)

9 References

[1] M. Punturo, *The Virgo sensitivity curve.* VIR-NOT-PER-1390-51.

[2] I. Fiori et al, *Seismic Noise Studies with run E2 data: a first attempt to monitor daily variation*, VIR-NOT-FIR-1390-212, 2002.

[3] R. Flaminio et al, *Advanced Virgo White paper*, VIR-NOT-DIR-1390-304 (2005).

[4] F. Piergiovanni, M. Punturo and P. Puppo, *The thermal noise of the Virgo+ and Virgo Advanced Last Stage Suspension (The PPP effect),* Virgo Note VIR-015C-09, 2009.

[5] Bernardini A., Majorana E. ,Puppo P. ,Rapagnani P. , Ricci F., Testi G. *Suspension last stages for the mirrors of the Virgo interferometric gravitational wave antenna.*, Rev. Sci. Instr. 70, no. 8 (1999): 3463.

[6] G. Cagnoli and P.A. Willems, *Effects of nonlinear thermoelastic damping in highly stressed fibers*., Phys. Rev. B, 65, 174111.

[7] G. Cagnoli et al, Rev. Sci. Instr., 69, 2777-2780, 1998.

[8] S. Frasca et al, *Electromagnetic coupling dissipation between mirrors and reaction masses in Virgo,* Phys. Lett. A, 252, 11116, 1999.

[9] P. Rapagnani, *Detector Report – STAC, November 10th 2009.*

[10] P. Puppo, *FEM of the strain energy stored in the Hydroxide-Catalysis Bonded ears of the mirrors for Virgo+*, VIR-XXX-09, in preparation.

[11] Andri M. Gretarsson and Gregory M. Harry, *Dissipation of mechanical energy in fused silica fibers*, Rev. Sci. Instr., 70, 10, 1999

[12] Andri M. Gretarsson et al, *Pendulum mode thermal noise in advanced interferometers: a comparison of fused silica fibers and ribbons in the presence of surface loss,* Phys, Lett. A, 270, 108-114, 2000.

[13] Gregory M. Harry *et al, Mechanical loss of laser-welded fused silica fibers.* Rev.Sci.Instr., Vol. 77, 023906, 2006.

[14] G. Cagnoli et al, Phys. Lett. A, 255, 230, 1999

[15] G. Cagnoli et al, Rev.Sci.Instr. 71, 2206, entry 18 of Table I.

[16] S.D.Penn et al, *Frequency and surface dependence of the mechanical loss in fused silica* Physics Letters A, 352, 3-6, 2006,.

[17] L. Cunningam, C. Torrie, A. Cumming. *Development of model for AdLIGO thermal noise simulation* LIGO-T080163-06.

[18] V.B. Braginsky et al., Phys. Lett. A , 264, 1-10, 1999

[19] V.B. Braginsky, S.P. Vyatchanin, Phys. Lett. A, 312, 2003.
[20] H.J.Kimble et al., Classical and Quantum Gravity, 19, 897-2012, 2002.
[21] F. Bondu, *Dark fringe shot noise sensitivity*. VIR-NOT-OCA-1390-243, 2003.
[22] Y. Levin, Phys. Rev. D, 57 (2), 659-663 (1998).
[23] Low Temperature-Elastic Moduli, Debye Temperature and Internal Dilational and Shear frictions of Fused Quartz.[Journal of Materials Science,32,(1997),1207-1211] Mikio Fukuhara, Asao Sanpei.
[24] M. Fukuhara and A. Sanpei, ISIJ International, vol 33(4), p508 (1993) and J.A. Rayne and B.S. Chandrasekhar, Physical Review, v122, p1714 (1961)
[25] Quartz Glass for Optics Data and Properties, Heraeus data sheet, numbers for suprasil.